Chemical Science

ROYAL SOCIETY OF CHEMISTRY

EDGE ARTICLE

View Article Online
View Journal | View Issue

Cite this: *Chem. Sci.*, 2025, **16**, 4101

All publication charges for this article have been paid for by the Royal Society of Chemistry

Received 30th September 2024
Accepted 16th January 2025

DOI: 10.1039/d4sc06631f

rsc.li/chemical-science

Thermal-responsive luminescence/dielectric responses with reversibly shifted light emissions†

Ming Zhu,‡[a] Pei-Zhi Huang,‡[a] Lin-Mei Li,[a] Yi-Xuan Yang,[a] Lei Pan,[a] Zhi-Jie Wang,[b] Hao-Fei Ni,[a] Feng-Wen Zhang,[a] Gele Teri,[a] Zhi-Xu Zhang,[a] Zunqi Liu,*[c] Da-Wei Fu*[ab] and Yi Zhang *[a]

Molecular-rotor-type crystals dominated by crown ethers have garnered significant attention for their applications in sensing, optoelectronics, information encryption and other diverse fields. However, the role of crown ethers in regulating photoluminescent properties has long been overlooked in such structural systems. Here, by inserting 18-crown-6 molecules into the ionic crystal (4-pyridinemethaneaminum)PF_6 (PP-1), we constructed a molecular-rotor-type crystal [(4-pyridinemethaneaminum)(18-crown-6)][PF_6] (PCP-1), exhibiting sensitively thermal-driven, unusual PL/dielectric responses. Notably, the introduction of the 18-crown-6 molecule changed the dynamic thermal motion and exerted a confinement effect through rich hydrogen bonding interactions, thereby inducing structural phase transitions and modulating energy transfer processes. These not only brought about switchable dielectric responses but also resulted in a comprehensive improvement of PL properties, encompassing extended lifetime, doubled quantum yield and temperature-controllable luminescent color. This study offers novel insights into the role of crown ethers in developing smart luminescent materials, holding promising prospects for intelligent recognition and information encryption.

Introduction

Crown ethers, discovered by Pedersen, are well-known cyclic organic compounds composed of repeating oligo-ethylene oxide units arranged in a ring array.[1] The annular cavities of crown ethers, with variable diameters, allow them to selectively bind to various components through heteroatoms as connection sites, making them useful in organic synthesis, ion separation, sensing, and other applications.[2–6] In host–guest chemistry, crown ethers can coordinate with almost all types of metal cations, enabling fascinating functions.[7–11] For example, Feldmann *et al.* assembled a series of 18-crown-6 coordinated metal halides with super-bright luminescence and nonlinear optical effects.[12] Our group achieved and directly observed slip ferroelectricity in a two-dimensional crystal (15-crown-5) Cd_3Cl_6.[13] Besides direct coordination with metal ions, crown ethers are also capable of loosely connecting with organic components through weak molecular interactions, forming a so-called molecular rotor system.[14–18] Under external energy fields, this structural model is prone to triggering rotational/swinging or local twisting motions, thereby inducing thermal, mechanical and electrical responses related to molecular orientation dynamics. These effects have been demonstrated in a series of works, such as [(*m*-FAni)(DB-18-crown-6)][Ni(dmit)$_2$],[19] [(CF_3-C_6H_4-NH_3)(18-crown-6)][TFSA][20] and [(*N*,*N*-dimethylethylenediammonium)(18-crown-6)]BF_4.[21] However, in contrast to the rich metal–organic coordination chemistry, little is known about the PL properties of crown-ether molecular rotor systems.

PL characteristics with special response capabilities have aroused great interest for potential applications in lighting, encryption, anti-counterfeiting, sensing, and other fields.[22–28] In the past few years, many works have been devoted to regulating PL properties such as lifetime, quantum yield, light colour, as well as their responsiveness to external stimuli.[29–33] What particularly attracts us is the temperature control of PL along with its relatively simple and easy to operate characteristics for widespread application. A typical example is the thermally controlled PL temporary quenching behaviour in the recently reported hybrid (*N*,*N*-dimethylmorpholinium)$_2$$MnBr_4$ for information encryption.[34] Equally important, thermal

[a]*Institute for Science and Applications of Molecular Ferroelectrics, Key Laboratory of the Ministry of Education for Advanced Catalysis Materials, Zhejiang Normal University, Jinhua 321004, People's Republic of China. E-mail: yizhang1980@seu.edu.cn*

[b]*Ordered Matter Science Research Center, Jiangsu Key Laboratory for Science and Applications of Molecular Ferroelectrics, Southeast University, Nanjing 211189, People's Republic of China. E-mail: dawei@zjnu.edu.cn*

[c]*Chemistry and Chemical Engineering College, Xinjiang Agricultural University, Urumqi 830052, People's Republic of China. E-mail: lzq@xjau.edu.cn*

† Electronic supplementary information (ESI) available: Experimental and computational details, crystal structure and PXRD images, PDOS results, crystallographic data. CCDC 2378751–2378756. For ESI and crystallographic data in CIF or other electronic format see DOI: https://doi.org/10.1039/d4sc06631f

‡ These authors contributed equally.

stimulation can also drive and integrate responses in other physical properties, enabling multifunctionality, especially through the multiple responses and possible interactions of optical/electrical channels.[35–42] The crown-ether-based molecular rotor structure also serves as an ideal platform for designing thermally driven dielectric responses.[43–46] The abundant hydrogen bonding between components in the molecular rotor system acts like ropes that pull and restrict each other, together with the inherently facile motion of crown ethers, which is beneficial for energy capture, transfer and conversion. Nevertheless, the role of crown ethers in regulating PL properties has long been overlooked in such molecular rotors, making these systems more challenging to study.

As the most widely applied crown ether, 18-crown-6 with a ring-opening diameter of ~300 pm provides an optimal cavity to accommodate the $-NH_3$ group of organic components.[47] In this work, by introducing 18-crown-6 molecules into the parent PP-1, we successfully constructed a molecular rotor-type compound PCP-1. Excitingly, the introduction of crown ethers not only brings about switchable dielectric response but also enables a comprehensive improvement of PL properties including lifetime extension, doubled quantum yield and temperature controllability of the luminescent colour (Scheme 1). Systematic characterization and calculations reveal that the addition of crown ethers exerts a confinement effect through abundant hydrogen bonding interactions, thereby promoting structural phase transition and modulating the energy transfer process.

Results and discussion

Structural and molecular interactions analysis

Colourless transparent crystals of PP-1 and PCP-1 were prepared by the slow evaporation of their respective mixed solution. Single crystal X-ray diffraction (SC-XRD) determinations were performed to reveal their crystal structures (Table S1†). At 303 K, PP-1 crystallizes in the monoclinic space group $P2_1/c$, with the asymmetric unit consisting of a 4-pyridinemethaneaminum (4-PDMA) cation and a PF_6^- anion. Structurally, 4-PDMA and PF_6^- are arranged alternately, which is stablished by N–H···N hydrogen bonds between N atoms of adjacent 4-PDMA and N–H···F hydrogen bonds between N atoms of 4-PDMA and F atoms of PF_6^- (Fig. 1(a) and Table S2†). The introduction of 18-crown-6 molecules into PP-1 induces an alteration in the crystal symmetry, leading to the crystallization of PCP-1 in the monoclinic space group $P2_1/n$, with the asymmetric unit of PCP-1 transitioning into an 18-crown-6 molecule, a 4-PDMA cation and a PF_6^- anion. Compared with the parent PP-1, the introduction of 18-crown-6 molecules changes the intermolecular hydrogen bonding from N–H···F and N–H···N to N–H···O, causing 4-PDMA cations to be anchored within the cavities of 18-crown-6 molecules and forming a molecular rotor-type structure (Fig. 1(b) and Table S3†). Meanwhile, PF_6^- anions are stabilized in the structure through weak molecular interactions, including P–F···H, P–F···C and P–F···O (Fig. S1†). Among them, P–F···H, P–F···C and P–F···O account for 97.5%, 2.3% and 0.2%, respectively. The molecular interactions in the crystal structures, especially the hydrogen bonds, not only affect the structural symmetry but also play a significant role in the physical properties. Based on the crystallographic data, the Hirshfeld surfaces of PP-1 and PCP-1 were calculated using the CrystalExplorer software package. With the 4-PDMA cations as the analytical center, for PP-1, two distinct red spots were observed in Fig. 1(c), which corresponded to the presence of two kinds of hydrogen bonding forces. Among these, N–H···N and N–H···F hydrogen bonds dominate in the Hirshfeld surfaces, and the average d_{norm} of the total Hirshfeld surfaces is 0.4908. For PCP-1, the red spots in Fig. 1(d) represent N–H···O hydrogen bonds, and the average d_{norm} of total Hirshfeld surfaces is 0.4881, smaller than that of PP-1, meaning stronger molecular interactions, which promote the fluorescent property of PCP-1 (see below). Meanwhile, the crystal structure of PCP-1 and PP-1 clearly reveals that the introduction of 18-crown-6 molecules changes the arrangement relationship between 4-PDMA cations and PF_6^- anions. Then, we used PF_6^- as the central ion to calculate the Hirshfeld surfaces (Fig. 1(e) and (f)). The calculated results show that the P–F···H hydrogen bonds dominate in the Hirshfeld surfaces, and the value of d_{norm} in PCP-1 (0.5404) is much larger than that in PP-1 (0.2980), indicating weaker molecular interactions surrounding PF_6^- in PCP-1 and lower energy barriers for molecular dynamic movement, thus facilitating molecular motion to some extent.

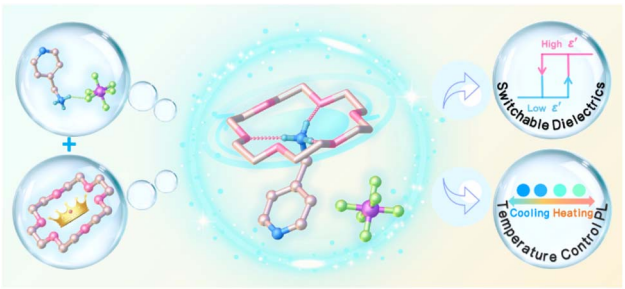

Scheme 1 Schematic design concept of PCP-1 switchable dielectrics and temperature-controlled PL response.

Phase transition and mechanism analysis

Based on the analysis of molecular interactions and the fact that crown ethers are temperature-sensitive,[48] we infer that PCP-1 may possess a temperature-dependent structural phase transition. Differential scanning calorimetry (DSC) determinations, as a direct and effective method to detect whether compounds undergo structural phase transitions, were conducted to verify this hypothesis. As illustrated in Fig. 2(a), a pair of reversible thermal anomalies was clearly observed at 428/394 K during heating/cooling runs with a thermal hysteresis of 34 K, indicating that PCP-1 possesses reversible structural phase transition. However, PP-1 did not undergo structural phase transition before its melting point. Based on the equation $\Delta S = \Delta H/T$, the average entropy (ΔS) value calculated for PCP-1 is 45.60 J mol^{-1} K^{-1}. Subsequently, according to the Boltzmann equation $\Delta S = R\ln(N)$ (where R is the ideal gas constant and N is the number of

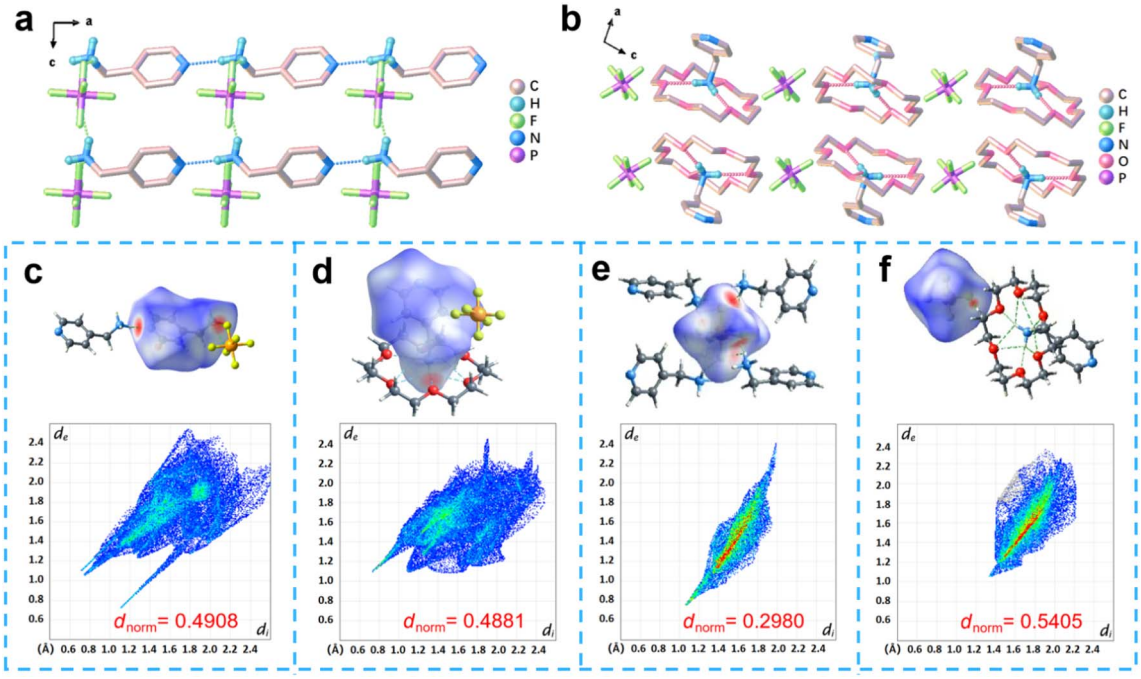

Fig. 1 (a and b) Packing structure of PP-1 (a) and PCP-1 (b) viewed along the crystallographic *b*-axis at 303 K. Pink and blue dashed lines indicate hydrogen bonds, with some hydrogen atoms omitted for clarity. (c and d) Hirshfeld d_{norm} surfaces and associated 2D fingerprint plots of the 4-PDMA cations in PP-1 (c) and PCP-1 (d). (e and f) Hirshfeld d_{norm} surfaces and associated 2D fingerprint plots of the PF_6^- anions in PP-1 (e) and PCP-1 (f).

geometrically distinguishable orientations), the value of N was calculated as 241.01. A large value of N means that the molecules will exhibit violent motion and high disorder after the high-temperature phase transition. For convenience, the phases below and above the phase transition temperature are labelled as the low temperature phase (LTP) and high temperature phase (HTP), respectively.

Despite many attempts and extensive efforts to obtain the HTP structure of PCP-1, the limited quality of SC-XRD data at high temperature has hindered the acquisition of a complete

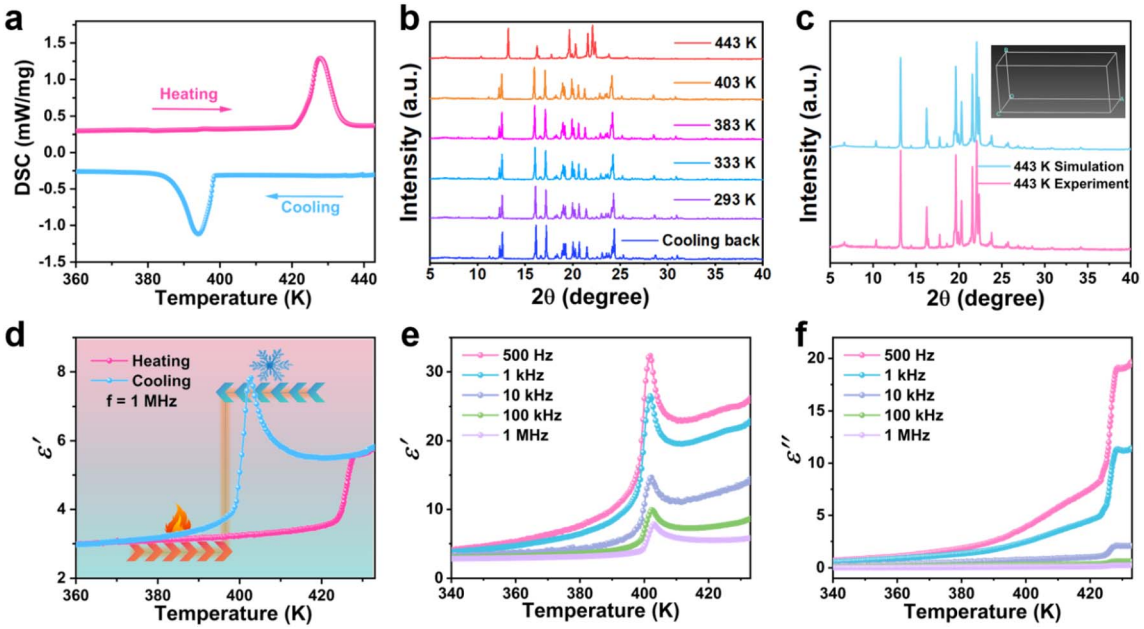

Fig. 2 (a) DSC curves of PCP-1 during heating and cooling cycles. (b) Variable-temperature PXRD patterns of PCP-1 during gradual heating from 293 K to 443 K and cooling back to 293 K. (c) Experimental and theoretical simulated patterns for PCP-1 at 443 K. (d) ε' curve of PCP-1 during heating and cooling cycles at 1 MHz frequency and schematic of a dielectric switch. (e) ε' curve of PCP-1 during the cooling process at different frequencies. (f) ε'' curve of PCP-1 during the heating process at different frequencies.

crystal structure. Therefore, variable-temperature powder X-ray diffraction (PXRD) measurements were further conducted to prove the reversible phase transition and infer the structure of PCP-1 at HTP. As shown in Fig. 2(b), the diffraction patterns of PCP-1 remained consistent within the temperature range from 293 K to 403 K, which also match well with the one simulated from the SC-XRD data at LTP, confirming the phase purity of PCP-1 (Fig. S2†). As the temperature increased to 443 K (above T_P), the diffraction peaks at $2\theta = 11.15°$, 12.25°, 12.51°, 15.96°, 17.08°, 18.82°, 19.89°, 20.57°, 21.25°, 24.11°, 25.17°, 28.46°, 30.27° and 34.46° either shifted, disappeared or decreased sharply, exhibiting the structural change of PCP-1. When the temperature dropped back to 293 K, both the number and location of peaks returned to the initial state. This phenomenon proves the reversible phase transition of PCP-1. In addition, with the PXRD data at 443 K, we further employed theoretical calculations to fit the cell parameters of PCP-1 to obtain the structural information at HTP. The fitted parameters were $\alpha = \gamma = \beta = 90°$, $a = 26.5930(7)$ Å, $c = 9.0410(8)$ Å, $b = 10.7854(9)$ Å, and $V = 2593.1(5)$ Å^3, which basically match the cell parameters derived from the SC-XRD determination. The fitting results indicate that PCP-1 in HTP belongs to the orthorhombic crystal system (*mmm* point group), and the most probable space group is *Pccn*. As illustrated in Fig. 2(c), the PXRD patterns of PCP-1 fitted through theoretical calculations match well with the measured one, validating the accuracy of the fitting results. To further reveal the mechanism of phase transition, we measured the crystal structures of PCP-1 at several gradually increasing temperatures before the phase transition (Table S4†). By comparison, it was found that the elliptic volume of 18-crown-6 molecule shows a continuous expansion as the temperature increases from 303 K to 423 K, similar to the change in 4-PDMA cations (Fig. S3 and Table S5†). Therefore, we inferred that the structural phase transition of PCP-1 can be attributed to the order–disorder type transitions of the 18-crown-6 molecule and 4-PDMA cations.

Dielectric constant (ε), as an important parameter that characterizes the degree of a material's response to an electric field, is sensitive to the change in the crystal structure and can be calculated according to the formula $\varepsilon = \varepsilon' - i\varepsilon''$ (where ε' represents the real part and ε'' represents the imaginary part of the dielectric constant). We further performed dielectric tests on the polycrystalline powder of PCP-1, and a pair of reversible dielectric anomalies appeared during the heating and cooling processes (Fig. 2(d)). As the temperature rises, the value of the real part of the dielectric constant (ε') shows a rapid stepwise increase at about 428 K, while during the cooling process, it drops sharply at about 394 K. PCP-1 demonstrates a temperature-responsive dielectric switch, exhibiting switchable dielectric states throughout the heating and cooling cycles. Meanwhile, the dielectric constant exhibits frequency dependence, as evidenced by the increase in its value from 8 to 32 when the measurement frequency decreases from 1 MHz to 500 Hz (Fig. 2(e)). Besides, as shown in Fig. 2(f), the value of ε'' also exhibits an obvious numerical variation near the phase transition temperature, with higher values observed at lower frequencies. The frequency-dependent dielectric response of PCP-1 renders it highly promising for applications in frequency-regulated dielectric switches.

Optical properties

The introduction of 18-crown-6 not only brings about phase transitions for PCP-1 but also endows the crystal with fascinating variations in its optical properties. Both PP-1 and PCP-1 crystals appear colourless under natural light, while they exhibit blue luminescence at room temperature when exposed to commercial ultraviolet light (365 nm) (Fig. S4†). The solid-state UV-vis absorption spectra at room temperature for PP-1 and PCP-1 were measured, as shown in Fig. S5.† The absorption spectra of PP-1 and PCP-1 exhibit distinct peaks at approximately 252 and 260 nm, respectively, suggesting that the introduction of 18-crown-6 does not significantly alter the absorption range. Additionally, through the steady-state photoluminescence (PL) spectrum measurements of the two crystals, the excitation wavelengths of PCP-1 and PP-1 were 393 nm and 353 nm, respectively, which can be attributed to the π–π* and n–π* transitions of 4-PDMA. Among them, the introduction of 18-crown-6 in PCP-1 results in a partial transfer of electrons from the 4-PDMA cations to 18-crown-6 molecules, leading to a relaxation of electron distribution and a reduction in the energy of the excited state. As a result, the fluorescence excitation wavelength of PCP-1 is greater than that of PP-1. The emission peaks measured at the corresponding excitation wavelengths were 455 nm for PCP-1 and 434 nm for PP-1, with Stokes shifts ($\Delta\lambda = \lambda_{em} - \lambda_{ex}$) of 62 nm and 82 nm, respectively (Fig. 3(a) and (b)). According to the equation $\tau_{ave} = \tau_1 a_1 + \tau_2 a_2$, the average decay lifetime (τ_{ave}) of emission light for PCP-1 was calculated to be 1.489 ns, nearly twice that of PP-1 (0.798 ns) (Fig. 3(c) and (d)). Additionally, the quantum yield of PCP-1 was 35.49%, significantly larger than that (18.21%) of PP-1 (Fig. 3(e) and (f)). Compared with the parent PP-1, the introduction of 18-crown-6 promotes the comprehensive luminescence performance of PCP-1, including luminescence intensity, fluorescence lifetime and quantum yield.

The luminescence properties of compounds are not only closely related to the luminophores themselves but also influenced by the surrounding molecular interactions, especially hydrogen bonding forces. The molecular motion of luminophores can be effectively restricted by hydrogen bonds, thereby promoting fluorescence emission.[49,50] For PCP-1, the introduction of 18-crown-6 results in the anchoring of 4-PDMA cations in their cavities. Hirshfeld surface calculations reveal that the value of d_{norm} for PCP-1 is 0.4881, which is smaller than the value of 0.4908 for PP-1, indicating a stronger molecular interaction surrounding the 4-PDMA cations in PCP-1 compared to PP-1. Therefore, the dynamic motion of 4-PDMA cations in PCP-1 is restricted, leading to an enhancement in fluorescence emission intensity, an increase in quantum yield and a prolongation of the emission lifetime.

To further probe the fluorescent properties of PP-1 and PCP-1, we measured their temperature-dependent PL spectra within the range of 303–443 K (Fig. 4(a) and (b)). It could be observed that the PL intensity of both the compounds gradually

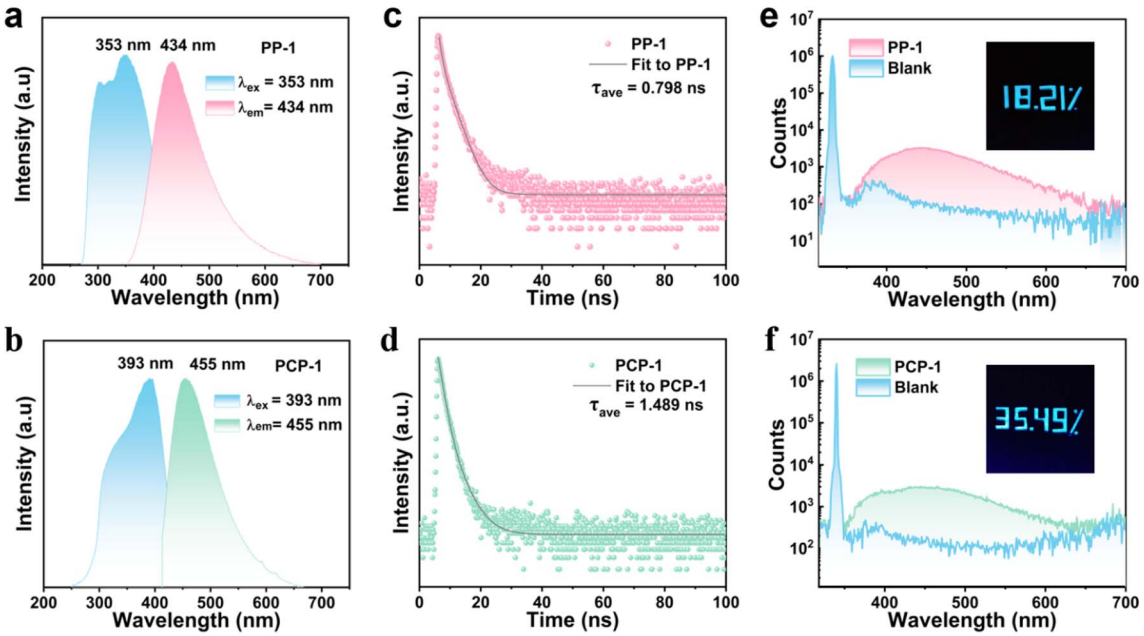

Fig. 3 (a and b) Excitation and emission spectra of PP-1 (a) and PCP-1 (b) at room temperature. (c and d) Time-resolved decay curves of PP-1 (c) and PCP-1 (b) crystals monitored at 353 nm. (e and f) Fluorescence quantum yields measured at room temperature for PP-1 (e) and PCP-1 (f).

decreases with increasing temperature, which can be attributed to the temperature-induced enhancement of lattice vibration and subsequent relaxation of the luminescent center. This results in an increased probability of non-radiative transitions and a reduction in luminescent intensity. As shown in the Fig. S3,† by comparing the crystal structures at different temperatures, it was found that as the temperature rises, the ellipsoidity of the molecules gradually increases, proving the intensification of lattice vibrations. More interestingly, an anomalous temperature-responsive PL is also observed in PCP-1. As the temperature increases from 303 K to 443 K, the emission peak of PCP-1 shifts from 455 nm to 511 nm and the coordinate points on the CIE chromaticity diagram (Fig. 4(c)) also shift from (0.1907, 0.218) to (0.2784, 0.3947), indicating a change in emitted colour with increasing temperature.

To validate the aforementioned measured data, we performed a heating and cooling cycle on the PCP-1 crystal on a heating platform and recorded the experimental phenomena

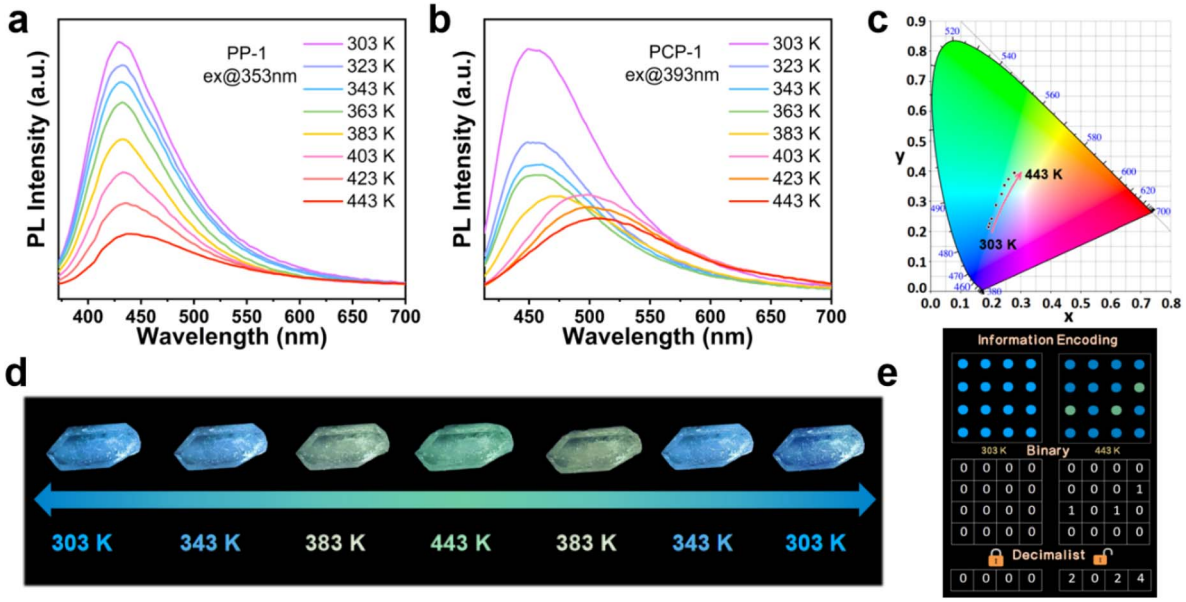

Fig. 4 (a) Temperature-dependent PL spectra (λ_{ex} = 353 nm) of PP-1. (b) Temperature-dependent PL spectra (λ_{ex} = 393 nm) of PCP-1. (c) Temperature-dependent CIE chromaticity coordinates of PCP-1. (d) Temperature-dependent luminescent colour of the PCP-1 crystals. (e) Schematic of the information encryption and decryption process based on the temperature-dependent PL responses of PP-1 and PCP-1.

in a dark environment under a 365 nm UV lamp. As depicted in Fig. 4(d), as the temperature increased, the PL colour gradually transitioned from blue to green, and upon cooling, the colour returned to blue. The observed phenomenon further substantiates the temperature controllability of luminescent colour in PCP-1 and confirms its reversibility, which is caused by the confinement effect of 18-crown-6 (see the part of DFT calculations). The performance of temperature-dependent luminescence holds significant potential for applications in diverse fields, including materials science, environmental monitoring, and optical encryption. As shown in Fig. 4(e), we designed an encryption strategy by pairing PP-1 and PCP-1. In this encryption model, it is defined that blue light corresponds to output code "0" while green light corresponds to output code "1". The encryption and decryption process as follows: under UV irradiation, the model composed of two substances emits blue fluorescence at a temperature of 303 K, converting the binary code to decimal, with each column corresponding to the invalid information "0". When the temperature rises to 443 K, part of the material emits green light, converting each column of digits to decimal and revealing the code "2024". Upon cooling back to room temperature, the blue fluorescence is restored, thus re-encrypting the information.

Density functional theory (DFT) calculations

To elucidate the comprehensive enhancement of PCP-1's luminescent performance and the temperature-controllable fluorescence emission mechanism, we conducted an investigation into the electronic structure and energy conversion of PCP-1 and parent PP-1. Based on first-principle, density functional theory (DFT) theoretical calculation was performed to obtain the partial density of states (PDOS) and the total density of states (DOS) of PCP-1 and PP-1, as well as the distribution of the highest occupied molecular orbital (HOMO) and lowest unoccupied molecular orbital (LUMO) orbital. The PDOS calculation for PCP-1 shows that the C 2p orbital contributes to the conduction band minimum (CBM) while the H 1s, O 2p, and N 2p orbitals contribute to the valence band maximum (VBM) (Fig. S6a†). For PP-1, Fig. S6b† indicates that the CBM is derived from the H 1s orbital while the VBM is contributed by C 2p and N 2p orbitals. Comparing with the parent PP-1, it was clearly found that the O 2p orbitals of the 18-crown-6 ring in PCP-1 is involved in electronic transfer. Furthermore, the electronic distributions of the LUMO and HOMO at 303 K in the two compounds are depicted in Fig. 5(a)–(d), revealing that the PF_6^- anion does not participate in the electron transfer process in either of the two compounds. In PP-1, both LUMO and HOMO are located on the 4-PDMA cations, indicating that the electrons are predominantly confined within the 4-PDMA cations. However, in PCP-1, the LUMO is localized on the 4-PDMA cations while the HOMO is situated on 18-crown-6. Therefore, the introduction of 18-crown-6 facilitates electron transfer between 4-PDMA cations and 18-crown-6 molecules, leading to a unique alteration in the electronic distribution. This distinctive change in electron distribution significantly affects the luminescent properties of PCP-1. Consequently, PCP-1 demonstrates an elevated fluorescence quantum yield, extended lifetime, and intensified emission intensity.

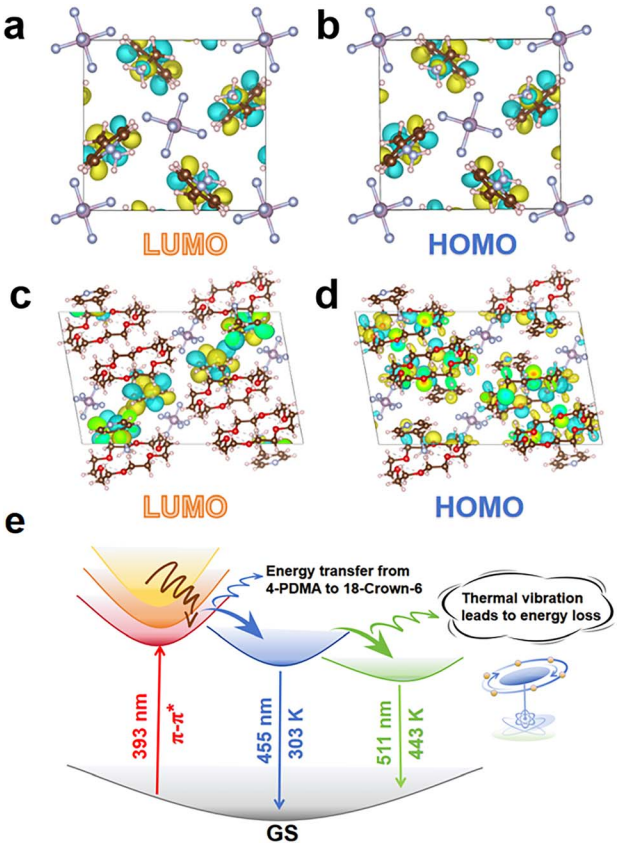

Fig. 5 (a–d) Theoretically calculated molecular orbitals of PP-1 (a and b) and PCP-1 (c and b). (e) Schematic of the molecular structure of PCP-1 at high temperatures and the photophysical scheme in the PL processes for PCP-1.

Additionally, as illustrated in Fig. 5(e), the 18-crown-6 molecules progressively absorb more energy with increasing temperature, initiating thermally-activated dynamic motion of the molecular rotor structure in PCP-1. Throughout the heating process, a portion of the excited-state energy is dissipated through vibrational relaxation, converting into thermal energy and consequently leading to a reduction in the energy of the excited state. This reduction in excited-state energy results in a decline in the emitted energy back to the ground state, manifesting as a redshift in the emission peak towards longer wavelengths. Also, the values of $d_{i\ min}$ and $d_{e\ min}$ for N–H···O hydrogen bonding in PCP-1 were calculated at different temperatures (Fig. S7†), where $d_{i\ min}$ and $d_{e\ min}$ represent the closest distance of the inner and outer atoms to the surface, respectively. The results demonstrate a decrease in both $d_{i\ min}$ and $d_{e\ min}$ values with increasing temperature, indicating a strengthening of hydrogen bonding between 4-PDMA cations and 18-crown-6. This change facilitates energy transfer between 4-PDMA cations and 18-crown-6, leading to a gradual increase in heat dissipation through the vibration of 18-crown-6 molecules, ultimately resulting in a decrease in fluorescence

intensity and redshifted photoluminescence of PCP-1 as the temperature rises. This intriguing temperature-dependent luminescence behaviour not only uncovers the complex optical mechanisms in crown ether systems but also offers a fresh perspective for exploring their unique optical properties.

Conclusions

In conclusion, we have synthesized a molecule rotor-type crystal PCP-1 through the introduction of 18-crown-6 molecules into the parent PP-1, realizing both phase transition and enhancement of photoluminescence performance. The introduction of 18-crown-6 alters the hydrogen bonding interactions and reorganizes the components in PCP-1, greatly reducing the molecular interactions surrounding the PF_6^- ions, thereby inducing phase transition behavior. Meanwhile, 4-PDMA cations are anchored in the cavity of 18-crown-6, regulating electron transfer during the photoluminescent process and resulting in an overall improvement in the photoluminescent performance of PCP-1. In particular, the distinctive temperature-controlled luminous colour behavior of PCP-1 holds promising potential for applications in information encryption. This successful example provides a reliable route to search for crystals with unique optical properties through constructing molecule rotor-type systems and finally reaching the aim of commercial optoelectronic applications.

Data availability

The data supporting this study are available in the ESI.†

Author contributions

M. Z.: conceived the idea, designed the experiments, analysed data, and wrote the manuscript. P.-Z. H.: assisted in the analysis of the data and revised the manuscript. H.-F. N.: performed the DFT calculations. F.-W. Z., L.-M. L., L. P., G. T., Y.-X. Y. and Z.-J. W.: assisted with the data collection and analysis. Z.-X. Z.: supervision and writing – review & editing. Z. L., D.-W. F. and Y. Z.: supervision, funding acquisition, project administration and writing – review & editing.

Conflicts of interest

There are no conflicts of interest to declare.

Acknowledgements

This work was financially supported by the National Natural Science Foundation of China (22405243, 22375182 and 22371258), and the Natural Science Foundation of Zhejiang Province (LZ24B010003 and LQN25B010003).

References

1 C. J. Pedersen, *J. Am. Chem. Soc.*, 1967, **89**, 7017–7036.
2 Y. Xia, Z. Song, Z. Tan, T. Xue, S. Wei, L. Zhu, Y. Yang, H. Fu, Y. Jiang, Y. Lin, Y. Lu, A. L. Ferguson and J. Cheng, *Nat. Commun.*, 2021, **12**, 732.
3 T. Ye, H. Gao, Q. Li, N. Liu, X. Liu, L. Jiang and J. Gao, *Angew. Chem., Int. Ed.*, 2024, **63**, e202316161.
4 N. Schuewer and H.-A. Klok, *Adv. Mater.*, 2010, **22**, 3251–3255.
5 H. Ju, Z. Yin, Z. Demchuk, V. Bocharova, C. Gainaru, J. A. Laub, K. Vogiatzis, R. Advincula, J. Chen and P.-F. Cao, *Adv. Funct. Mater.*, 2024, **34**, 2402165.
6 T.-S. Su, F. T. Eickemeyer, M. A. Hope, F. Jahanbakhshi, M. Mladenović, J. Li, Z. Zhou, A. Mishra, J.-H. Yum, D. Ren, A. Krishna, O. Ouellette, T.-C. Wei, H. Zhou, H.-H. Huang, M. D. Mensi, K. Sivula, S. M. Zakeeruddin, J. V. Milić, A. Hagfeldt, U. Rothlisberger, L. Emsley, H. Zhang and M. Grätzel, *J. Am. Chem. Soc.*, 2020, **142**, 19980–19991.
7 L. Li, K. Kang, T.-S. Chee, Z. Tian, Q. Sun and C. Xiao, *Adv. Sci.*, 2024, **11**, 2308663.
8 G. Yang, X. Liu, L. Wang, K. Dong, B. Zhang, X. Jiang, Y. Yin, M. Wang, W. Niu, L. Zheng, S. Yu, S. Liu, S. M. Zakeeruddin, X. Guo, S. Pang, L. Sun, M. Gratzel and M. Wei, *Angew. Chem., Int. Ed.*, 2024, e202410454.
9 P. W. Fritz, T. Ashirov and A. Coskun, *Chem*, 2024, **10**, 2207–2219.
10 Z. Wang, J.-T. Mo, J.-J. Pan and M. Pan, *Adv. Funct. Mater.*, 2023, **33**, 2300021.
11 W.-J. Xu, Q.-C. Luo, Z.-H. Li, Y.-Q. Zhai and Y.-Z. Zheng, *Adv. Sci.*, 2024, **11**, 2308548.
12 E. Merzlyakova, S. Wolf, S. Lebedkin, L. Bayarjargal, B. L. Neumeier, D. Bartenbach, C. Holzer, W. Klopper, B. Winkler, M. Kappes and C. Feldmann, *J. Am. Chem. Soc.*, 2021, **143**, 798–804.
13 L.-P. Miao, N. Ding, N. Wang, C. Shi, H.-Y. Ye, L. Li, Y.-F. Yao, S. Dong and Y. Zhang, *Nat. Mater.*, 2022, **21**, 1158–1164.
14 W. Li, C.-T. He, Y. Zeng, C.-M. Ji, Z.-Y. Du, W.-X. Zhang and X.-M. Chen, *J. Am. Chem. Soc.*, 2017, **139**, 8086–8089.
15 Y.-F. Gao, Z.-X. Zhang, T. Zhang, C.-Y. Su, W.-Y. Zhang and D.-W. Fu, *Mater. Chem. Front.*, 2020, **4**, 3003–3012.
16 X.-J. Song, T. Zhang, Z.-X. Gu, Z.-X. Zhang, D.-W. Fu, X.-G. Chen, H.-Y. Zhang and R.-G. Xiong, *J. Am. Chem. Soc.*, 2021, **143**, 5091–5098.
17 W. Li, D.-X. Liu, W.-Y. Hu, Q.-Y. Liu, Z.-Y. Du, C.-T. He, W.-X. Zhang and X.-M. Chen, *Chin. J. Chem.*, 2022, **40**, 1917–1923.
18 M.-M. Lun, C.-Y. Su, Q.-Q. Jia, Z.-X. Zhang, J. Li, H.-F. Lu, Y. Zhang and D.-W. Fu, *Inorg. Chem. Front.*, 2023, **10**, 5026–5034.
19 T. Akutagawa, H. Koshinaka, D. Sato, S. Takeda, S.-I. Noro, H. Takahashi, R. Kumai, Y. Tokura and T. Nakamura, *Nat. Mater.*, 2009, **8**, 342–347.
20 H.-P. Lv, Y.-R. Li, X.-J. Song, N. Zhang, R.-G. Xiong and H.-Y. Zhang, *J. Am. Chem. Soc.*, 2023, **145**, 3187–3195.
21 M. M. Lun, J.-Q. Luo, Z.-X. Zhang, J. Li, L.-Y. Xie, H.-F. Lu, Y. Zhang and D.-W. Fu, *Chem. Eng. J.*, 2023, **475**, 145969.
22 M. Chen, C. Ye, C. Dai, R. Qi, H. Fu, C. Luo, H. Peng and H. Lin, *Adv. Opt. Mater.*, 2022, **10**, 2200278.

23 Y. Fan, X. Jin, M. Wang, Y. Gu, J. Zhou, J. Zhang and Z. Wang, *Chem. Eng. J.*, 2020, **393**, 124799.
24 G. Xiao, Y.-J. Ma, Z. Qi, X. Fang, T. Chen and D. Yan, *Chem. Sci.*, 2024, **15**, 3625–3632.
25 Y. Xue, Y. Chen, G. Li, W. Xia, Q. Mao, L. Pei, M. Liu, L. Chu and J. Zhong, *Chin. Chem. Lett.*, 2024, **35**, 108447.
26 P.-C. Chen, A. P. Periasamy, S. G. Harroun, W.-P. Wu and H.-T. Chang, *Coordin. Chem. Rev.*, 2016, **320**, 129–138.
27 Y. Tai, R. Cui, J. Zhang, C. Wang, T. Zhao, B. Zhang and C. Deng, *J. Rare Earths*, 2024, **42**, 1458–1469.
28 X. Hou, C. Ke, C. J. Bruns, P. R. McGonigal, R. B. Pettman and J. F. Stoddart, *Nat. Commun.*, 2015, **6**, 6884.
29 V. Morad, S. Yakunin and M. V. Kovalenko, *ACS Mater. Lett.*, 2020, **2**, 845–852.
30 P. Wei, X. Zhang, J. Liu, G.-G. Shan, H. Zhang, J. Qi, W. Zhao, H. H. Y. Sung, I. D. Williams, J. W. Y. Lam and B. Z. Tang, *Angew. Chem., Int. Ed.*, 2020, **59**, 9293–9298.
31 H. Zhao, Q. Wang, Z. Wen, H. Sun, S. Ji, X. Meng, R. Zhang, J. Jiang, Z. Tang and F. Liu, *Angew. Chem., Int. Ed.*, 2023, **62**, e202316336.
32 S. Wang, Y. Yao, Z. Wu, Y. Peng, L. Li and J. Luo, *J. Mater. Chem. C*, 2018, **6**, 12267–12272.
33 C. Zhu, J. Jin, Z. Wang, Z. Xu, M. C. Folgueras, Y. Jiang, C. B. Uzundal, H. K. D. Le, F. Wang, X. Zheng and P. Yang, *Science*, 2024, **383**, 86–93.
34 M.-M. Lun, H.-F. Ni, Z.-X. Zhang, J.-Y. Li, Q.-Q. Jia, Y. Zhang, Y. Zhang and D.-W. Fu, *Angew. Chem., Int. Ed.*, 2024, **63**, e202313590.
35 H. Li, Y. Li, L. Zhang, E. Hu, D. Zhao, H. Guo and G. Qian, *Adv. Mater.*, 2024, 2405535.
36 X. Han, P. Cheng, S. Han, Z. Wang, J. Guan, W. Han, R. Shi, S. Chen, Y. Zheng, J. Xu and X.-H. Bu, *Chem. Sci.*, 2024, **15**, 3530–3538.
37 M. Maczka, M. Ptak, A. Gagor, D. Stefanska and A. Sieradzki, *Chem. Mater.*, 2019, **31**, 8563–8575.
38 D. Ren, L. Tang, Z. Wu, Q. Zhang, T. Xiao, R. B. P. Elmes and L. Wang, *Chin. Chem. Lett.*, 2023, **34**, 108617.
39 M. Rok, B. Zarychta, A. Bil, J. Trojan-Piegza, W. Medycki, A. Miniewicz, A. Piecha-Bisiorek, A. Cizman and R. Jakubas, *J. Mater. Chem. C*, 2021, **9**, 7665–7676.
40 J. Harada, T. Fujiwara and K. Ogawa, *J. Am. Chem. Soc.*, 2007, **129**, 16216–16221.
41 Q. Wang, J. Jin, Z. Wang, S. Ren, Q. Ye, Y. Dou, S. Liu, A. Morris, C. Slebodnick and L. Quan, *J. Am. Chem. Soc.*, 2024, **146**, 8971–8980.
42 W.-C. Qiao, H. Qiao, X. L. Wang, H. Xu, F. Xu, Z. Sun, H. Gao and Y.-F. Yao, *Small*, 2024, **20**, 2310529.
43 D.-W. Fu, W. Zhang, H.-L. Cai, Y. Zhang, J.-Z. Ge, R.-G. Xiong and S. D. Huang, *J. Am. Chem. Soc.*, 2011, **133**, 12780–12786.
44 Y. Zhang, H.-Y. Ye, D.-W. Fu and R.-G. Xiong, *Angew. Chem., Int. Ed.*, 2014, **53**, 2114–2118.
45 C.-R. Huang, Y. Li, Y. Xie, Y. Du, H. Peng, Y.-L. Zeng, J.-C. Liu and R.-G. Xiong, *Angew. Chem., Int. Ed.*, 2021, **60**, 16668–16673.
46 Y.-Z. Tang, Y.-M. Yu, J.-B. Xiong, Y.-H. Tan and H.-R. Wen, *J. Am. Chem. Soc.*, 2015, **137**, 13345–13351.
47 J. W. Steed, *Coordin. Chem. Rev.*, 2001, **215**, 171–221.
48 H.-Y. Ye, S.-H. Li, Y. Zhang, L. Zhou, F. Deng and R.-G. Xiong, *J. Am. Chem. Soc.*, 2014, **136**, 10033–10040.
49 B.-H. Kim, W. Kim, T. Kim, B. M. Ko, S.-J. Hong, K. Lee, J. Kim, S.-H. Song and S. Lee, *ACS Appl. Mater. Interfaces*, 2021, **13**, 54339–54347.
50 S.-L. Deng, T.-L. Chen, W.-L. Chien and J.-L. Hong, *J. Mater. Chem. C*, 2014, **2**, 651–659.